Supplement of Hydrol. Earth Syst. Sci., 25, 6339–6357, 2021
https://doi.org/10.5194/hess-25-6339-2021-supplement

Hydrology and Earth System Sciences
Open Access
EGU

Supplement of

Quantifying the impacts of land cover change on hydrological responses in the Mahanadi river basin in India

Shaini Naha et al.

Correspondence to: Shaini Naha (sn17546@bristol.ac.uk)

S1 Root depth and fraction estimation approach in the VIC model

Typical implementation of VIC-3L model includes three soil layers and three root zones to represent soil moisture uptake through the plant roots. Depths and fractions of the root zones are user-defined for each land use types so that shorter vegetation draw soil moisture from the upper soil layer and deep-rooted plants from the deeper soil layers. VIC assumes that the roots are linearly distributed within the root zones and computes the root fractions for each soil layer by linear interpolation (Figure S1 left). Depths of soil layers are generally calibrated which requires the model to redistribute the user-defined root fractions specified for each root zone, in the soil layer by linear interpolation. Most of the studies related to VIC model have adopted this approach where the soil depths are calibrated and allocation of roots are kept constant (Demaria et al., 2007; Lilhare et al., 2020; Mishra et al., 2010; Park and Markus, 2014; Parr et al., 2015; Yeste et al., 2020). Demaria et al., (2007) tested the sensitivity of root distribution on the second soil layer in VIC-3L and found that different root allocations have impacted the ET and baseflow in the basin.

In this study we replace typical system of using fixed rooting depths and root fractions for varying soil depths in VIC model by determining the root allocations for the changed soil depths considering Zeng (2002) root distribution approach. We first obtained the effective rooting depth of each vegetation types from Zeng (2002). The three root zone depths add up to the effective rooting depth. For simplicity, we assumed that the depth of the root zones is same as the depth of the soil layer, in other words, if the effective rooting depth is exactly equal to the total soil depth, then each soil layer corresponds to each root zone. However, there may be cases where the effective rooting depth are less than the total soil depths, for example as in Figure S1 (right). In this case, third root zone depth (z3) is obtained after subtracting root depths of first two root zones (z1, z2) from the total rooting depth(z_r). Therefore, the root depths of each vegetation type in our approach are a function of effective rooting depth, that is kept fixed for each vegetation types, and the soil depths are subjected to change during calibration. Although the root depths are not subjected to SA in this study, causing change in rooting depths by this approach will have implications on the sensitivity of soil depths. Next, the root fractions for each land cover type is determined using Zeng (2002) vegetation root distribution approach.

$$f = 1 - \frac{1}{2}(e^{-az_r} + b^{-bz_r}) \quad \text{Eq (1)}$$

Where *f* is the cumulative root fraction from the surface to the effective root depth z_r. *a* and *b* are the vegetation coefficients that depend on the vegetation types. We used this equation directly to derive root fractions for each layer. The vegetation coefficients and the effective root depths used for the vegetation types are given in Table S1.

S2 Morris Sensitivity Analysis Method

Morris (1991) is a well-established and widely used global sensitivity analysis (GSA) methods. There are many studies that have conducted parameter sensitivity analysis for hydrological models based on Morris screening method (Herman et al., 2013; Huang et al., 2020; Pappenberger et al., 2008; Pianosi et al., 2015; Sarrazin et al., 2016, 2018; Wang and Solomatine, 2019). It is a global extension of One-factor-At-the-Time local SA method. It is based on estimation of several elementary effects. The *EE* of the i^{th} input factor, x_{i-1}, at a single baseline point and for a known perturbation Δ can be calculated as given below (Campolongo et al., 2011).

$$EE = \frac{y(x_1,x_2,\ldots,x_{i-1},x_i+\Delta,\ldots,x_m) - y(x_1,x_2,\ldots,x_{i-1},x_i,\ldots,x_m)}{\Delta} \quad \text{Eq (2)}$$

'*m*' is the total number of parameters subjected to sensitivity analysis and 'y' is EEs for each input parameter, which is estimated at 'r' (See Eq. 3) random baseline points across the input parameter space. The estimated mean (μ_i) of the EEs is a measure of total-order effects of the i^{th} input parameter and standard deviation (σ_i) indicates the interaction effects of i^{th} input factor with another.

Morris method in this study is implemented as follows:

1. We performed the computational experiments using the SAFE (SA For Everybody) Toolbox (Pianosi et al., 2015)
2. '*m*' denotes the number of factors (model input parameters) subjected to sensitivity analysis, which is 16 in our case.
3. We used the radial design strategy proposed by Campolongo et al., (2011) to define the baseline points and the perturbation Δ.
4. 'r' baseline points sampled across the input parameter space are generated by the Maximin Latin Hypercube Sampling.

5. In this method, total number of model simulations (N) required depends on the base sample size or the number of EEs (*r*) and number of parameters (*m*). It is worth mentioning that EET can be used for three purposes: parameter screening, parameter ranking and parameter mapping. And the choice of *r* depends on the purpose of EET. In this study, we are more interested in screening out the non-influential parameters. We choose r as 70, and the choice is made based on the recommendations in the existing literatures, where EET is used for screening purposes (Saltelli et al., 2008; Sarrazin et al., 2016; Vanuytrecht et al., 2014, Ruano et al., 2012).
6. Base sample size of *r* = 70 have resulted in over 1000 model evaluations (*N*):

$$N = r(m + 1) \qquad \text{Eq. (3)}$$

Next, we compute the sensitivity measures for each input factor (Eq. 4). To avoid the problems due to effects of opposite signs, we estimate the mean of the absolute values of elementary effects ($|EE_i|$) as proposed by (Campolongo et al., 2011)

$$\mu_i^* = \frac{1}{r}\sum_1^r |EE_i| \qquad \text{Eq. (4)}$$

S2.1 Screening of input parameters

The screening objective consists of separating the model input parameters into two distinct groups, parameters that are: influential (sensitive) and non-influential (insensitive) for streamflow simulation. There may be parameters with sensitivity index value, zero, which is completely insensitive. However, our goal is not only to screen out a completely insensitive parameters but also the parameters having small or negligible impact. We therefore assumed a threshold value for the sensitivity index, below which the parameters can be regarded as either completely insensitive or less influential (Eq. 5). This is a common practice followed in several studies while dealing with parameter screening using different SA methods (Gou et al., 2020; Sarrazin et al., 2016; Tang et al., 2007; Vanrolleghem et al., 2015).

$$X_0 = \{X_i \; when \; S_i < threshold\} \qquad \text{Eq. (5)}$$

Where X_0 is the non-influential parameter, X_i is the i^{th} input parameter and S_i is the sensitivity index (mean of EE, μ_i^*) of the i^{th} input parameter. The choice of screening threshold can be subjective depending on the screening objective and case-specific threshold value are usually used (Sarrazin et al., 2016; Vanuytrecht et al., 2014), however very little information exists on this topic in the literature (Vanrolleghem et al., 2015). In this study, we set a screening threshold of 0.05 based on the visual analysis of the sensitivity index values of all

factors at all subcatchments. We choose this threshold with the intention of screening out also the less sensitive parameters, apart from completely insensitive parameters with an aim of reducing the over-parameterization effects in the model. One should evaluate the SA results by assessing the screening convergence which can be assessed by quantifying the stability in the partitioning of sensitive and insensitive parameter as derived from Eq. 6. However, the results would then depend on the choice of threshold value which is not predefined. Therefore, to achieve a more objective screening convergence result, we compute the width of the 95% confidence interval of the sensitivity indices, estimated by the bootstrap method (Archer et al., 1997; Efron and Tibshirani, 1993), also followed in studies (Herman et al., 2013; Wang and Solomatine, 2019). We then use maximum width of the 95% confidence interval, as a statistic, across the lower influential input parameters, X_0 suggested by Sarrazin et al., (2016) shown in Eq. 6.

$$Stat_{Screen} = \max_{x_i \in x_0} S_i^{ub} - S_i^{lb} \qquad \text{Eq. (6)}$$

where S_i^{ub} and S_i^{lb} are the upper and lower bounds of the sensitivity index of the i^{th} input factor while *m* is the number of input factors. We consider screening convergence is reached, when $Stat_{Screen}$ value for the non-influential parameters (found in Eq. 6) is below 10% of the sensitivity index value of the most influential parameter. This is also followed in Herman et al., (2013) whereas Sarrazin et al., (2016), assessed convergence by directly using a threshold value. If the convergence is not reached for the lower influential parameters, it would require adding more samples to our previously chosen base sample size and run the model again and repeat this process again.

S2.2 Morris screening results

We first obtain the sensitivity indices for all the subcatchments shown in Figure S2. We apply Eq5 on all the subcatchments to obtain five different sets of X_0 i.e., five sets of less influential parameters. We notice that there is a common set of parameters (*binf, ds, dsmax, ws*) which is more influential across all five subbasins. Also, there is a common set of non-influential parameters (*Ksat, diff, d1, d3, bd,* r_{arc}). Although the resulting influential and non-influential parameters at the subcatchments are comparable, we see few parameters which might be slightly influential for one subbasin whereas non-influential for the others. For instance, parameters *Exp* and Wp_f are slightly above the threshold for Salebhata, whereas for other subbasins they are non-influential. Note that we cannot compare the sensitivity indices values

of the parameters among the subcatchments, as μ_i depends on scale of measurements of the model output, we can compare the order of the parameters only.

We realize there are no major differences in the sensitivity results of these subcatchments, hence we choose to obtain a single set of influential parameters for the whole basin and discard the rest (Figure S2). We compute the weighted average of the sensitivity indices of each subcatchment, and the weights are assigned based on the catchment area (Eq 7).

$$\mu_{i(wa)} = (A_{Ba}. \mu_i + A_{ka}* \mu_i + ... + A_{Sa}* \mu_i) / (A_{Ba} + A_{Ka} + ... + A_{Sa}) \quad \text{Eq (7)}$$

Where $\mu_{i(wa)}$ is the weighted average of the i_{th} input parameter; A_{Ba}, A_{ka} and A_{Sa} are the catchment areas of Basantpur, Kantamal and Salebhata, respectively. This also renders in huge computational savings while calibrating the model, which otherwise would have required separate calibration runs (calibrating different set of parameters) for each subbasin. We observe that the influential parameters obtained for the whole subbasin is dsmax, d2, binf, v, ws and ds, which is same as the common set of influential parameters obtained earlier for all the subbasins, with only one additional parameter, v. Convergence plot using a decreasing number of samples suggest that the convergence for the non-influential parameters (Figure S3) has reached before reaching the total number of simulations (1190 simulations) and that the total number of model simulations run for Morris screening method was sufficient. Figure S4 shows maximum width of the 95% confidence interval of all the parameters below 0.08 (10% of the sensitivity index value of the most influential input factors) are indicated by a red dotted line. It satisfies the criteria that we set in Eq 6: all the parameters that are considered non-influential in Fig S3 (right), $Stat_{Screen}$ values of those parameters (marked in red) are below 0.08.

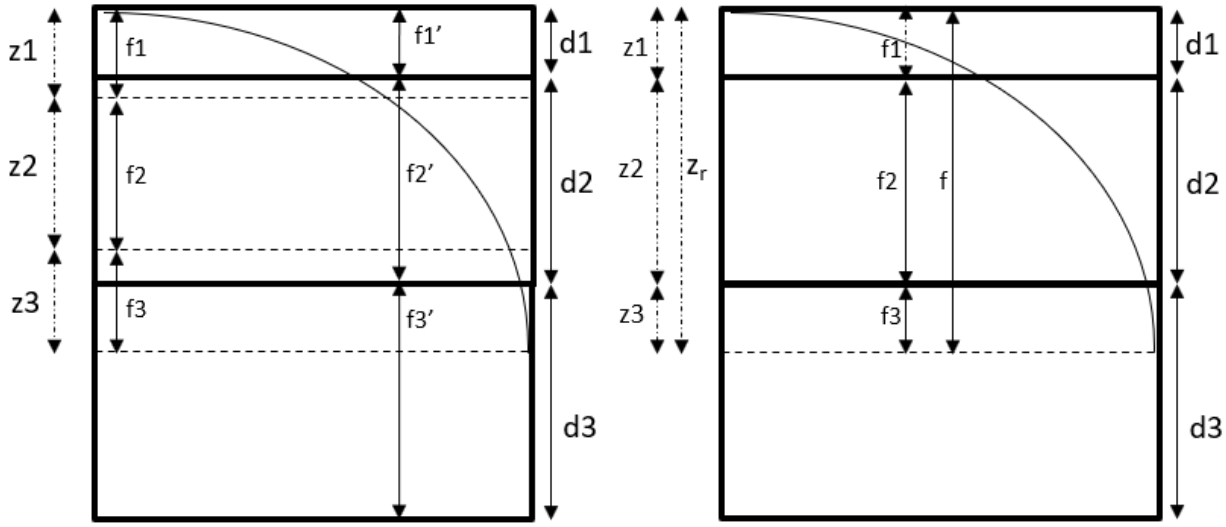

Figure S1: (left) Representation of rooting distributions in VIC-3l model. z1, z2 and z3 are the user-defined depths of three root zones, respectively. d1, d2, d3 are the depths of three soil layers. f1, f2 and f3 are user-defined fractions of root in each zone, respectively. f1', f2' and f3' are fractions of root in each soil layer computed by VIC. (right) Our approach of representation of rooting distributions in VIC-3L model. z_r is the total root depth.

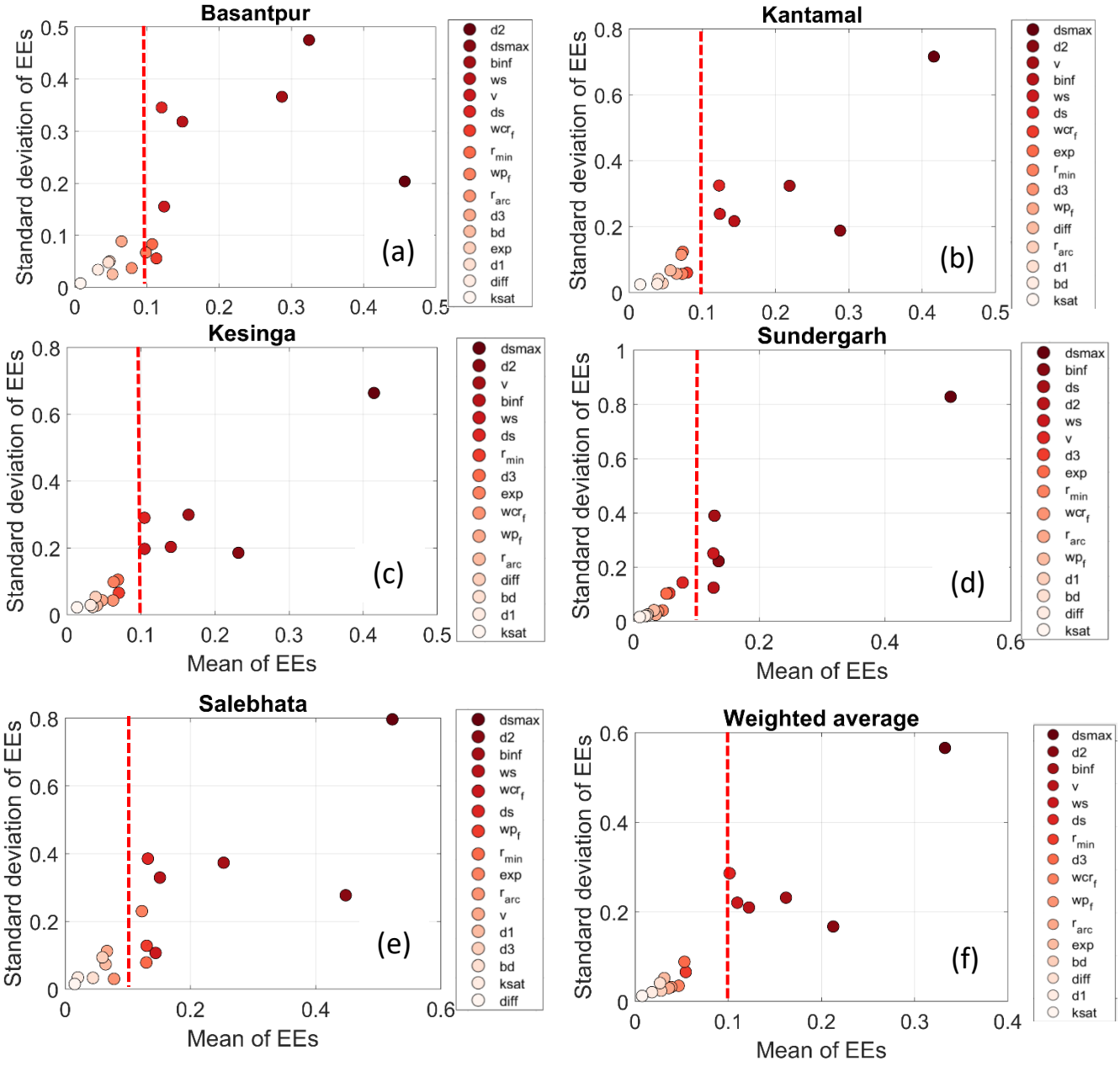

Figure S2: Sensitivity indices (Mean and Standard deviation) of Morris Method for VIC-3L parameters for (a-e) individual subbasins of Mahanadi river basin respectively (f) weighted average of all subcatchments. Parameters, top to bottom, listed on the right side are in ranking order, highest to lowest influential respectively, based on Mean of EEs. Red dashed vertical line is the screening threshold.

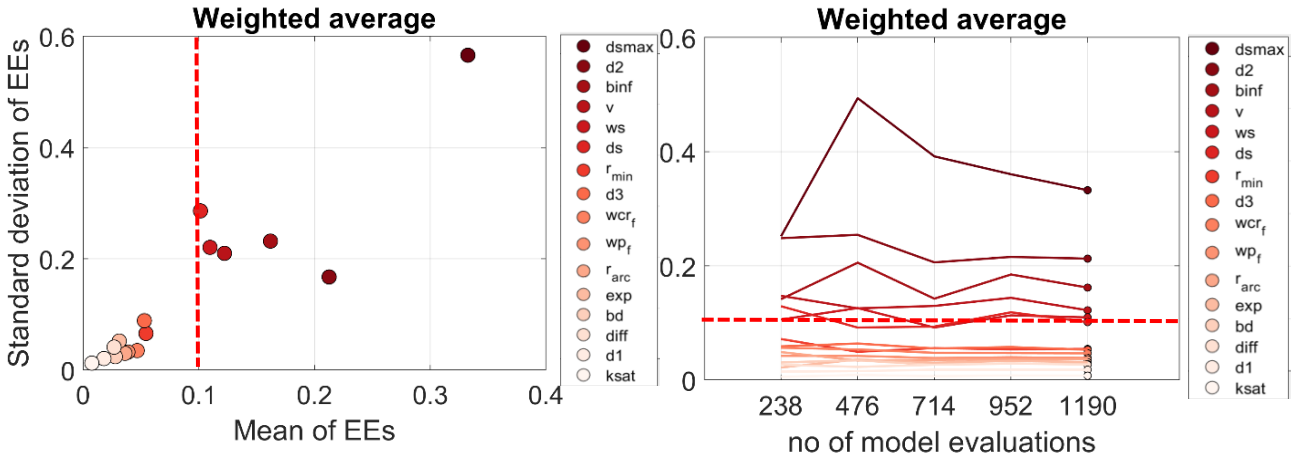

Figure S3: (left) Sensitivity indices (Mean and Standard deviation) of Morris Method for VIC-3L parameters for Mahanadi river basin (computed based on weighted average of all subbasins). (right) Convergence analysis using a decreasing number of samples. Red dashed horizontal/vertical line is the screening threshold. Parameters, top to bottom, listed on the right side are in ranking order, highest to lowest influential parameter respectively, based on Mean of EEs.

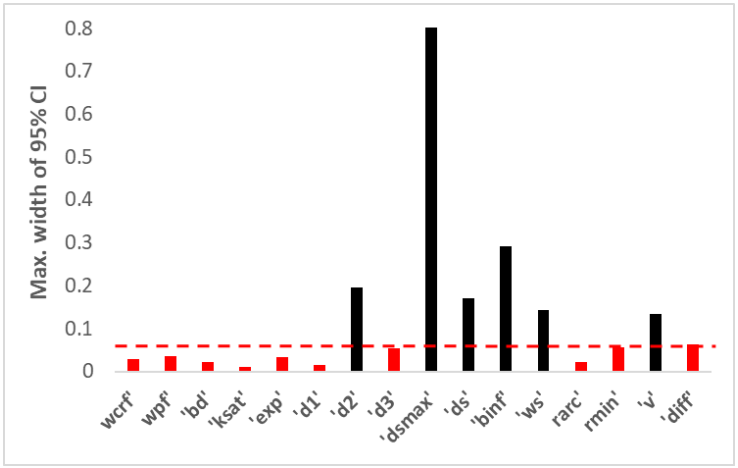

Figure S4: Maximum width of the 95% bootstrap confidence interval of all parameters. Dotted red line is the $Stat_{Screen}$ threshold, below which are the non-influential parameters that have converged.

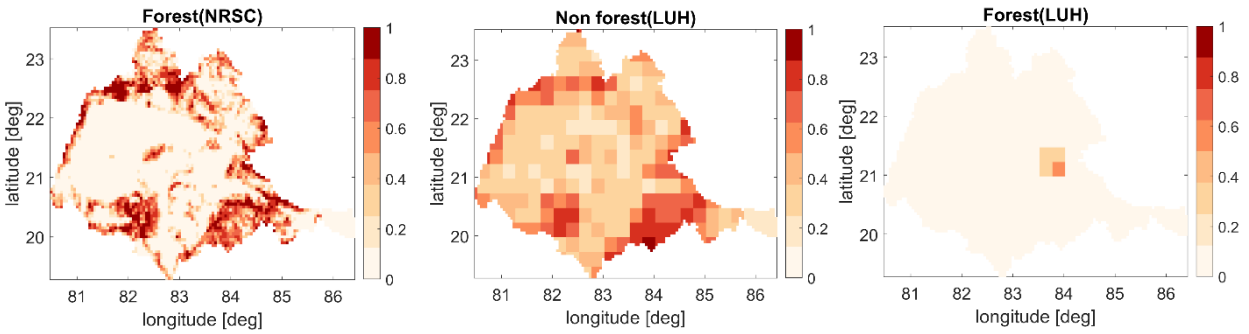

Figure S5 Forested areas in NRSC, 'Potential Non-Forested areas' in LUH2 and 'potentially forested areas' in LUH2. 'Potential Non-Forested areas' in LUH2 is comparable with the Forested areas in NRSC, through visual inspection. Therefore, both the 'potentially forested area' and 'potentially non-forested area' are combined and mapped as forest.

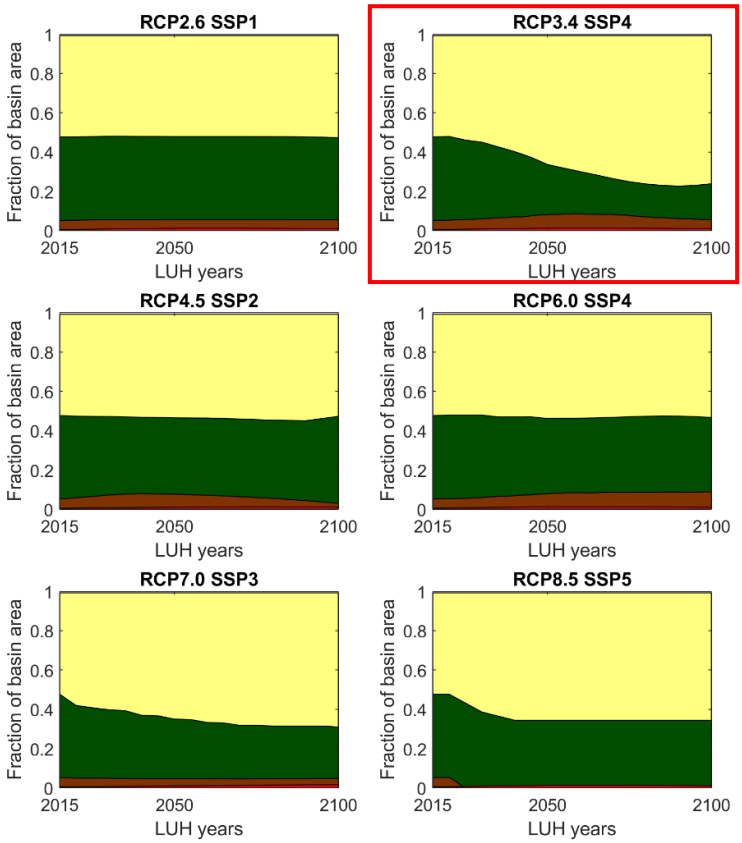

Figure S6 Land cover changes and fractional area covered in all LUH2 scenarios. Maximum changes are observed in RCP3.4 SSP4, hence selected as a 'worst case' scenario for simulating the hydrological impacts.

(a)

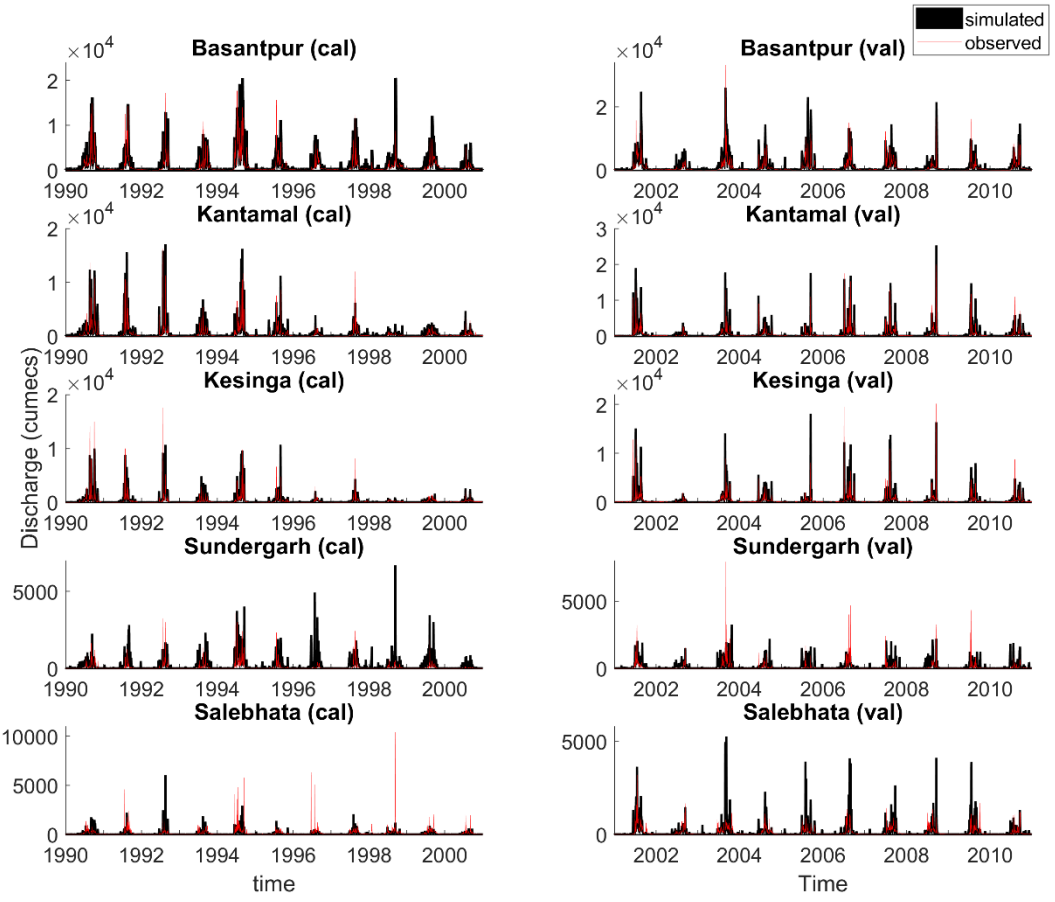
simulated
observed
Basantpur (cal)
Basantpur (val)
Kantamal (cal)
Kantamal (val)
Kesinga (cal)
Kesinga (val)
Sundergarh (cal)
Sundergarh (val)
Salebhata (cal)
Salebhata (val)
Discharge (cumecs)
time
Time

(b)

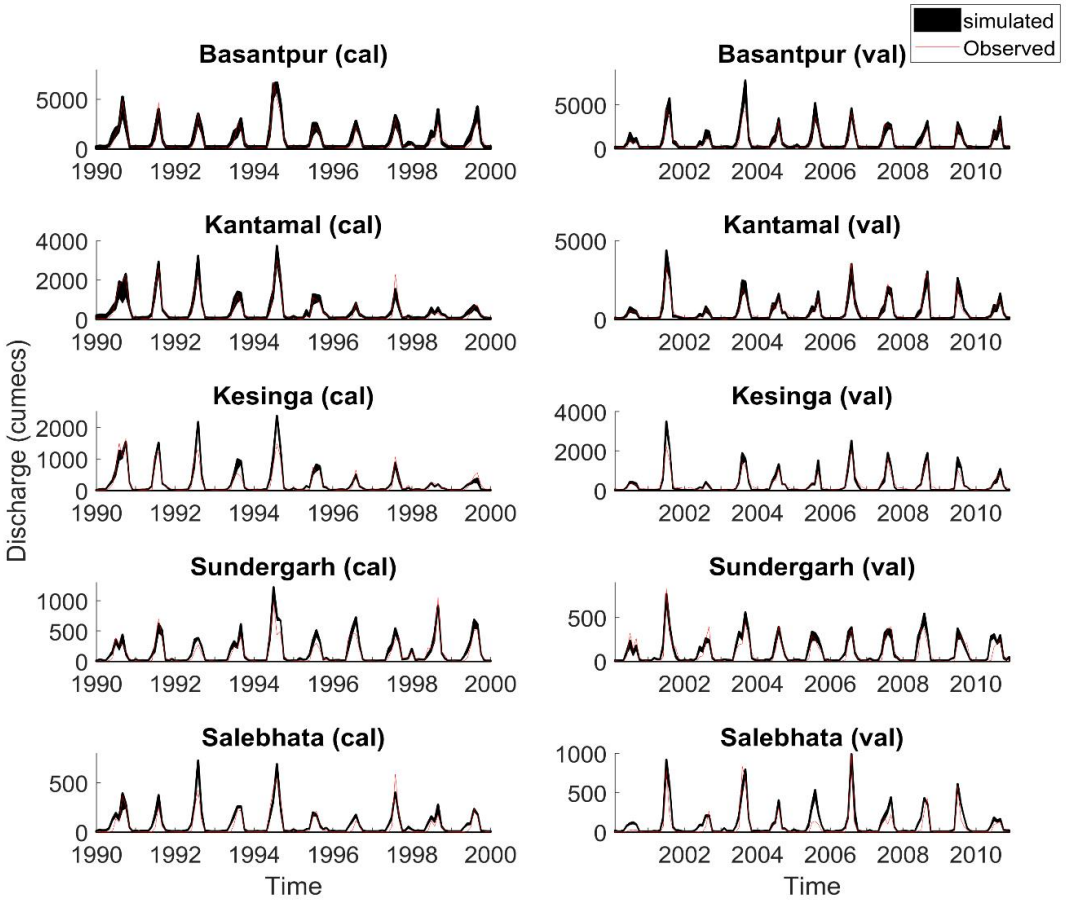
simulated
Observed
Basantpur (cal)
Basantpur (val)
Kantamal (cal)
Kantamal (val)
Kesinga (cal)
Kesinga (val)
Sundergarh (cal)
Sundergarh (val)
Salebhata (cal)
Salebhata (val)
Discharge (cumecs)
Time

Figure S7 Comparison between the measured and simulated (a) daily streamflow values (b) monthly streamflow values for the calibration and period at all subcatchments. Area highlighted in black represents the uncertainties in simulated streamflow arising from behavioral model parameter sets.

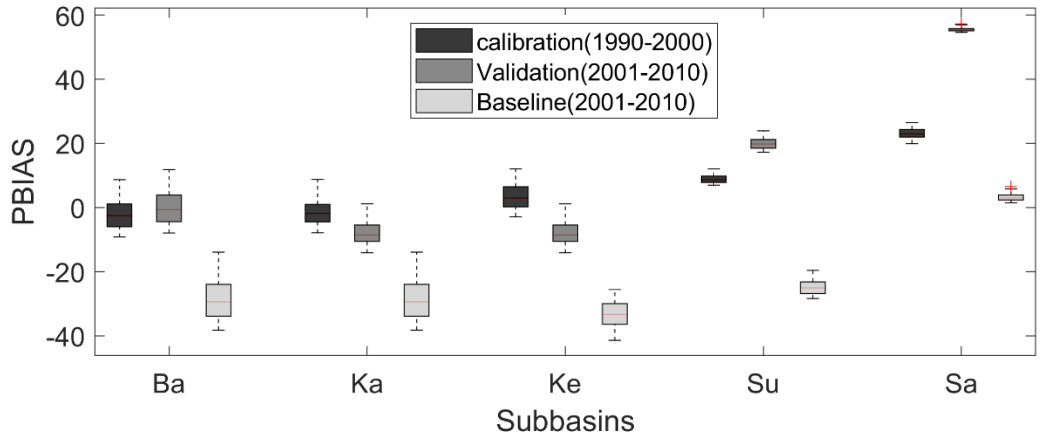

Figure S8 Percent bias plot of calibrated, validated and baseline simulations. Baseline simulations are the simulations using global land cover map from LUH2 of year 2005.

Table S1: Coefficients a and b in vegetation root distribution for Eq for the land cover types used in this study. The depth of the rooting zone zt is also given (Zeng, 2002)

Land cover type	a (m^{-1})	b (m^{-1})	z_t (m)
Deciduous broadleaf Forest	5.99	1.95	2
Cropland	5.56	2.61	1.5
Grassland	10.74	2.61	1.5
Open shrubland	7.72	1.26	3.1
Barren	4.37	0.98	4

Table S2 LUH2 future scenarios and models. These scenarios are the combination of RCP's projecting the magnitude and extent of climate change (Taylor et al., 2012; van Vuuren et al., 2011) and SSP'S (Hausfather, 2018) based on worlds of various levels of challenges to adaptation and mitigation (van Vuuren et al., 2014).

Scenarios	Models
RCP2.6 SSP1	IMAGE
RCP3.4 SSP4	GCAM
RCP4.5 SSP2	MESSAGE-GLOBIOM
RCP6.0 SSP4	GCAM
RCP7.0 SSP3	AIM
RCP8.5 SSP5	REMIND-MAGPIE

Table S3 LUH2 LULC classes remapped to VIC LULC cover classes.

LUH2	VIC
Forested primary land	Deciduous Broadleaf Forest (DBF)
Non forested primary land	Deciduous Broadleaf Forest (DBF)
Potentially forested secondary land	Deciduous Broadleaf Forest (DBF)
Potentially non-forested secondary land	Deciduous Broadleaf Forest (DBF)
Managed pasture	Grassland (GL)
Rangeland	Grassland (GL)
Urban land	Urban/built up (UB)
C3 annual crops	Cropland (CL)
C3 perennial crops	Cropland (CL)
C4 nitrogen-fixing crops	Cropland (CL)

Table S4 Range of KGE'S for the daily calibration and validation at all subcatchments.

Subcatchments	Calibration (1990-2000)	Validation (2001-2010)	Baseline (2001-2010)
Ba	0.83-0.88	0.70-0.83	0.54-0.75
Ka	0.85-0.88	0.76-0.88	0.54-0.73
Ke	0.81–0.84	0.65-0.76	0.50-0.65
Sa	0.74-0.76	0.55-0.67	0.58-0.67
Su	0.62-0.66	0.54-0.60	0.61-0.75

REFERENCES

Archer, G. E. B., Saltelli, A. and Sobol, I. M.: Sensitivity measures, anova-like techniques and the use of bootstrap, J. Stat. Comput. Simul., 58(2), 99–120, doi:10.1080/00949659708811825, 1997.

Campolongo, F., Saltelli, A. and Cariboni, J.: From screening to quantitative sensitivity analysis. A unified approach, Comput. Phys. Commun., 182(4), 978–988, doi:10.1016/j.cpc.2010.12.039, 2011.

Demaria, E. M., Nijssen, B. and Wagener, T.: Monte Carlo sensitivity analysis of land surface parameters using the Variable Infiltration Capacity model, J. Geophys. Res. Atmos., 112(11), 1–15, doi:10.1029/2006JD007534, 2007.

Efron, B. and Tibshirani, R. J.: Chapter 17: Cross-Validation, An Introd. to Bootstrap, 1993.

Gou, J., Miao, C., Duan, Q., Tang, Q., Di, Z., Liao, W., Wu, J. and Zhou, R.: Sensitivity Analysis-Based Automatic Parameter Calibration of the VIC Model for Streamflow Simulations Over China, Water Resour. Res., 56(1), 1–19, doi:10.1029/2019WR025968, 2020.

Hausfather, Z.: Analysis: How much 'carbon budget'is left to limit global warming to 1.5 C, Carbon Br., 9, 2018.

Herman, J. D., Kollat, J. B., Reed, P. M. and Wagener, T.: Technical Note: Method of Morris effectively reduces the computational demands of global sensitivity analysis for distributed watershed models, Hydrol. Earth Syst. Sci., 17(7), 2893–2903, doi:10.5194/hess-17-2893-2013, 2013.

Huang, J. B., Wen, J. wei, Wang, B. and Hinokidani, O.: Parameter sensitivity analysis for a physically based distributed hydrological model based on Morris' screening method, J. Flood Risk Manag., 13(1), 1–13, doi:10.1111/jfr3.12589, 2020.

Lilhare, R., Pokorny, S., Déry, S. J., Stadnyk, T. A. and Koenig, K. A.: Sensitivity analysis and uncertainty assessment in water budgets simulated by the variable infiltration capacity model for Canadian subarctic watersheds, Hydrol. Process., 34(9), 2057–2075, doi:10.1002/hyp.13711, 2020.

Mishra, V., Cherkauer, K. A., Niyogi, D., Lei, M., Pijanowski, B. C., Ray, D. K., Bowling, L. C.

and Yang, G.: A regional scale assessment of land use/land cover and climatic changes on water and energy cycle in the upper Midwest United States, Int. J. Climatol., 30(13), 2025–2044, doi:10.1002/joc.2095, 2010.

Morris, M. D.: Factorial sampling plans for preliminary computational experiments, Technometrics, 33(2), 161–174, 1991.

Pappenberger, F., Beven, K. J., Ratto, M. and Matgen, P.: Multi-method global sensitivity analysis of flood inundation models, Adv. Water Resour., 31(1), 1–14, doi:10.1016/j.advwatres.2007.04.009, 2008.

Park, D. and Markus, M.: Analysis of a changing hydrologic flood regime using the Variable Infiltration Capacity model, J. Hydrol., 515, 267–280, doi:10.1016/j.jhydrol.2014.05.004, 2014.

Parr, D., Wang, G. and Bjerklie, D.: Integrating Remote Sensing Data on Evapotranspiration and Leaf Area Index with Hydrological Modeling: Impacts on Model Performance and Future Predictions, J. Hydrometeorol., 16(5), 2086–2100, doi:10.1175/jhm-d-15-0009.1, 2015.

Pianosi, F., Sarrazin, F. and Wagener, T.: A Matlab toolbox for Global Sensitivity Analysis, Environ. Model. Softw., 70, 80–85, doi:10.1016/j.envsoft.2015.04.009, 2015.

Saltelli, A., Ratto, M., Andres, T., Campolongo, F., Cariboni, J., Gatelli, D., Saisana, M. and Tarantola, S.: Global sensitivity analysis: the primer, John Wiley & Sons., 2008.

Sarrazin, F., Pianosi, F. and Wagener, T.: Global Sensitivity Analysis of environmental models: Convergence and validation, Environ. Model. Softw., 79, 135–152, doi:10.1016/j.envsoft.2016.02.005, 2016.

Sarrazin, F., Hartmann, A., Pianosi, F., Rosolem, R. and Wagener, T.: V2Karst V1.1: A parsimonious large-scale integrated vegetation-recharge model to simulate the impact of climate and land cover change in karst regions., 2018.

Tang, Y., Reed, P., Wagener, T. and Van Werkhoven, K.: Comparing sensitivity analysis methods to advance lumped watershed model identification and evaluation, Hydrol. Earth Syst. Sci., 11(2), 793–817, doi:10.5194/hess-11-793-2007, 2007.

Taylor, K. E., Stouffer, R. J. and Meehl, G. A.: An overview of CMIP5 and the experiment design, Bull. Am. Meteorol. Soc., 93(4), 485–498, doi:10.1175/BAMS-D-11-00094.1, 2012.

Vanrolleghem, P. A., Mannina, G., Cosenza, A. and Neumann, M. B.: Global sensitivity analysis for urban water quality modelling: Terminology, convergence and comparison of different methods, J. Hydrol., 522, 339–352, doi:10.1016/j.jhydrol.2014.12.056, 2015.

Vanuytrecht, E., Raes, D. and Willems, P.: Global sensitivity analysis of yield output from the water productivity model, Environ. Model. Softw., 51, 323–332, doi:10.1016/j.envsoft.2013.10.017, 2014.

van Vuuren, D. P., Edmonds, J., Kainuma, M., Riahi, K., Thomson, A., Hibbard, K., Hurtt, G. C., Kram, T., Krey, V., Lamarque, J. F., Masui, T., Meinshausen, M., Nakicenovic, N., Smith, S. J. and Rose, S. K.: The representative concentration pathways: An overview, Clim. Change, 109(1), 5–31, doi:10.1007/s10584-011-0148-z, 2011.

van Vuuren, D. P., Kriegler, E., O'Neill, B. C., Ebi, K. L., Riahi, K., Carter, T. R., Edmonds, J., Hallegatte, S., Kram, T., Mathur, R. and Winkler, H.: A new scenario framework for Climate Change Research: Scenario matrix architecture, Clim. Change, 122(3), 373–386, doi:10.1007/s10584-013-0906-1, 2014.

Wang, A. and Solomatine, D. P.: Practical experience of sensitivity analysis: Comparing six methods, on three hydrological models, with three performance criteria, Water (Switzerland), 11(5), 1–26, doi:10.3390/w11051062, 2019.

Yeste, P., García-Valdecasas Ojeda, M., Gámiz-Fortis, S. R., Castro-Díez, Y. and Jesús Esteban-Parra, M.: Integrated Sensitivity Analysis of a Macroscale Hydrologic Model in the North of the Iberian Peninsula, J. Hydrol., 590(September 2019), 125230, doi:10.1016/j.jhydrol.2020.125230, 2020.

Zeng, X.: Global Vegetation Root Distribution for Land Modeling, J. Hydrometeorol., 2(5), 525–530, doi:10.1175/1525-7541(2001)002<0525:gvrdfl>2.0.co;2, 2002.